Joint Special Interest Group meeting between euspen and ASPE
Advancing Precision in Additive Manufacturing
KU Leuven, Belgium, September 2023
www.euspen.eu

Quantifying defect formation signatures in laser powder bed fusion through melt pool imaging and data-driven analysis

Sebastian Larsen[1], Paul A. Hooper[1]

[1]*Department of Mechanical Engineering, Imperial College London, UK*

sebastian.larsen16, paul.hooper@imperial.ac.uk

Abstract
Additive manufacturing (AM) processes, such as Laser-Powder Bed Fusion (L-PBF), require real-time quality assurance to mitigate defects. This study aims to elucidate defect signatures through image analysis and machine learning (ML). An experiment is devised to insert spatter defects in a controlled repeatable manner. The experiment is monitored with high-magnification and coaxial camera systems enabling the systematic investigation of spatter initiation and subsequent defect formation. The study also introduces an easy-to-implement interpretable ML tool that highlights key features associated with the coaxial images and detected defects. The results indicate that large spatter particles, on the order of 200 µm, can become airborne, interfere with the laser beam, and contaminate local surfaces. The formed defect could be detected by the coaxial system on the subsequent layer, with the most important feature being the integrated image intensity. The introduced methods enable effective quantification of defect predictions and facilitates a deeper understanding of defect formation mechanisms.

Data-driven, In-situ monitoring, Laser powder bed fusion, Machine learning, Melt pool imaging.

1. Introduction

Deployment of in-situ monitoring methods in Additive Manufacturing (AM) for mission-critical components could displace costly inspection methods such as micro-Computed Tomography (micro-CT) scanning, while enabling early detection of processing failures, saving significant costs in production and reducing waste. Yet challenges exist with handling the large quantities of data collected during processing. There is a need to automate the extraction of information for operators and stakeholders. Therefore, machine learning (ML) methods have been developed to mine important patterns from the data.

As the prevalence of ML techniques increases, there is a strong need to understanding the developed methods and how the predictions are made. This is necessary for two reasons. Firstly, the end user needs a way to interpret the results of predictions on physical terms. Highlighting and approach would allow the human operator to distinguish between a prediction error and a likely flaw. Secondly, there is a need for the research community to better understand the relationship between measurement and defect formation.

There has, recently, been a rapid adoption of ML methods in AM. This includes approaches that detect laser defocus [1], and surface discontinuities [2]. Multi-sensor fusion approaches combine sensors to enable improved detection of defects [3]. However, more work is needed understand the important predictive features and sensors, as well as the formation mechanisms, thereby enabling more robust defect localisation.

This study seeks to better understand the formation mechanisms of spatter defects as well as the important features needed to detect the defect. The paper begins with a description of the experimental setup. This is followed by the imaging methods, including the high-magnification and coaxial setups. The results section begins with a look at defect initiation, where the two systems are analysed. A detailed look at how the spatter defect forms a surface discontinuity is then explored. The detection of the defect on the subsequent layer is studied. Finally, the interpretable ML technique is deployed to understand which features were important in detecting the defect.

2. Methodology

2.1. Experiment

The experiment is shown in Fig. 1 and is designed to encourage the formation of spatter particle defects at B that will be transferred onto A due to the direction of shielding gas. The scan paths on B are altered to be aligned with the gas flow which encourages spatter to be transferred with the flow. The laser is also defocussed to encourage more spatter particles to form. The component is manufactured on a Renishaw AM250 L-PBF machine. Part A is built with nominal processing parameters (200W laser power, 60 µm pulse distance, 80 µs exposure time). The laser is defocussed by 15 mm on Part B. This is repeated four times within the build at separate height locations for a total of twelve layers. This encourages the build to return to nominal conditions before initiating further defects.

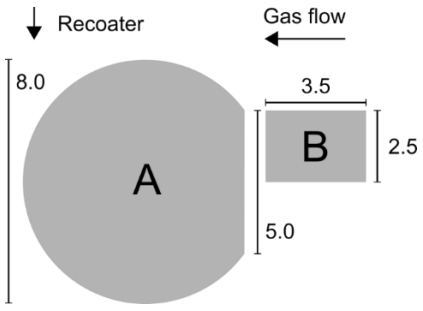

Figure 1. Experiment showing nominal main part A and neighbouring defect initiator, B. The laser has nominal build parameters in A and is defocussed in B to encourage spatter formation. Units in mm.

2.2. Imaging setups

Two camera systems are used to image the build in the present study. The high-magnification system is used to identify initiation and landing sites of spatter particle defects, while the coaxial system is used for detection.

The high-magnification imaging setup is shown in Fig. 2. The setup includes a zoom lens set to 12x magnification (Thorlabs MVL12X3Z). The optical train transmits light to a high-speed camera (Phantom Miro M310) imaging at 7,200 fps. A high-power blue LED is used to illuminate the imaging target, with light transmitted into the chamber using a liquid light guide.

Another high-speed camera is mounted coaxially (Phantom S200). The optical setup is modified from the previous system described in detail in [4]. The single camera system is capable of streaming continuously throughout the entire build and captures data at 20,000 fps. A near infrared (NIR) bandpass filter (950 nm) is placed in the optical train along with a Neutral Density filter.

Image features were extracted from the coaxial images with segmentation techniques. A threshold was set above the background noise and the melt pool was segmented along with spatter particles. Four features were then extracted. Firstly, the spot area, which is the high intensity region of the melt pool associated with the keyhole, was computed by taking a threshold at around 60% of the maximum. Secondly, the melt pool area was extracted which is area of the region above the background noise associated with the melt pool. The number of spatter particles were also counted. Finally, an intensity integral of the image was taken by computing a summation of total pixel intensity.

$$Integrated\ intensity = \sum_{i=1}^{m}\sum_{j=1}^{n} I_{ij}\ ,$$

where I_{ij} is the intensity of a pixel in row *i*, column *j*.

The features are input to an ML model. A Graph Neural Network was deployed to detect the defects, described in previous studies [5, 6]. The model takes both features as well as the positionally encoded laser scan paths. This allows both geometrical and imaging information to be fused. The model predictions are then converted to a voxel map of each layer. For the purposes of this study, a single layer and single defect are analysed to determine the important features leading to the prediction of the defect.

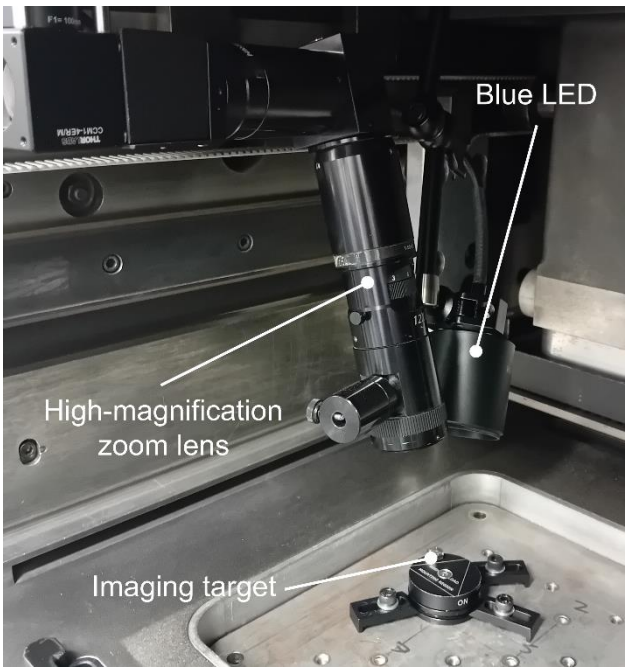

Figure 2. High-magnification imaging setup for the experiment.

3. Results and discussion

3.1. Defect initiation

A large spatter particle is captured from the imaging systems is shown in Fig. 3. The defect is initiated in the very first track of part B. The first track is particularly susceptible to defects as powder is entrained from both sides of the track. Combined with the defocus of the laser, this results in the formation of balling defects. Some of the particles can become airborne. Due to the large surface tension of the liquid metal, the melted particles combine and are flung into the air in a slingshot fashion as previously melting material, which has not yet solidified, tugs backwards on the melt pool imparting momentum on the system. The particle ascends vertically at an angle into the gas flow. The laser passes back and forth on the track, interacting twice with the particle. However, as the gas flow acts against the particle, it changes direction and is transferred onto the neighbouring part A, where it lands on the surface as a large balling flaw.

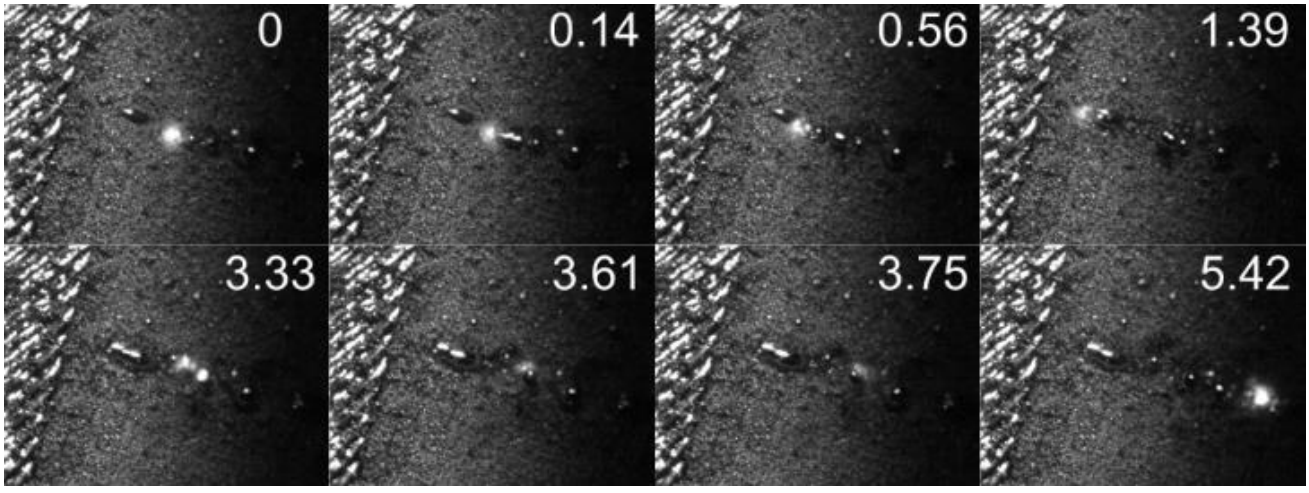

Figure 3. The initial formation of a large spatter particle from 0 to 1.39 ms as the laser scans the first track of part B. The particle becomes airborne and proceeds to interfere with the laser from 3.33 to 3.75 ms as the laser returns for the second scan track, leaving a void.

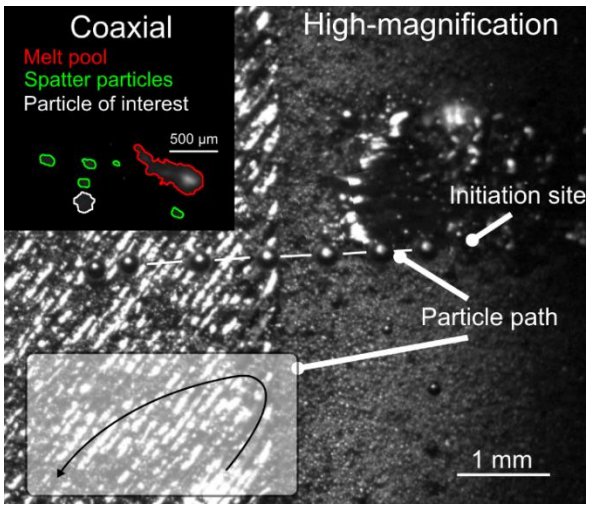

Figure 4. A large spatter particle path captured by each imaging system. The particle remains airborne for around 61 ms.

The trajectory of the particle can be seen in Fig. 4. The particle was also visible in the coaxial images (inset of Fig. 4). Since the particle is airborne for several scan track traversals (a total of 61 ms), there was also a tendency to observe interaction with the laser. Additionally, many more smaller particles also readily contaminated the neighbouring part.

Therefore, this type of defect is of particular interest as it has two failure modes. Firstly, it can interfere with the laser energy input, therefore potentially causing localised lack-of-fusion. Secondly, as the particles are large (around 200 µm), they pose significant risk of surface contamination, therefore, interfering with the melting process on the proceeding layers. A total of five defects form in this manner over the twelve layers (41.6%) suggesting the method is repeatable yet maintains the stochastic nature of a process induced flaw. Such events are relevant to geometries that are close by on the build plate meaning there is an increased risk of cross-contamination.

3.2. Defect detection and interpretation

The coaxial data for the subsequent layer was also analysed for anomalies. The detection map determined from the coaxial imaging system is shown in Fig. 5, overlaid on the landing site of the spatter particle. The particle had a strong influence on the scanning tracks on the next layer that contributed to variation beyond the particle itself, as can be seen by the larger detection region.

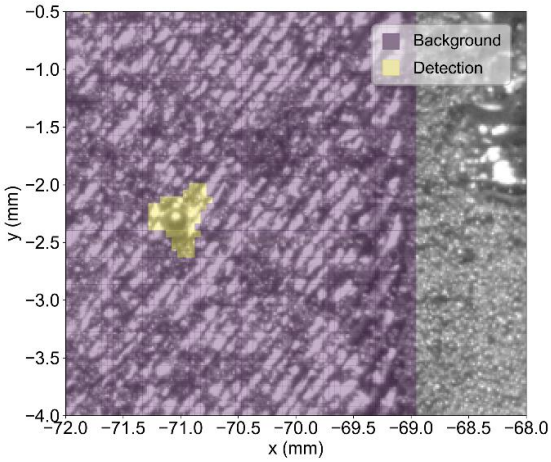

Figure 5. Prediction map of the subsequent layer overlaid onto the previous layer where the surface defect can be observed.

To better quantify how the particles were detected, a permutation feature importance measure was computed [7]. To determine the score, each feature was randomly permuted individually. The importance of the feature was then determined by how much the performance reduced. In this case, the performance was measured by taking the number of detections within a 100 µm radius of the defect. The detection at baseline was 100%, therefore the error was measured in relation to this for each feature.

The result is shown in Fig. 6. The intensity integral was by far the most important with an average 77% performance drop when this feature was permuted. This is followed by spot area at 4%, melt pool area at 1% and spatter number at 0%. The result suggests that little spatter forms during interaction with the particle but that there is a significant loss in intensity.

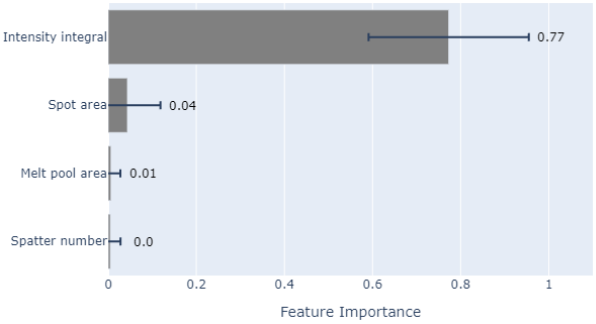

Figure 6. The most influential features were computed with a permutation feature importance method.

4. Conclusion

In this study, an approach to create spatter defects was verified through both high-magnification and high-speed coaxial imaging. The formation of a large spatter particle of approximately 200 µm was observed as multiple smaller particles combined. Two failure mechanisms were observed. Firstly, the spatter particle interfered with the laser and secondly contaminated a nearby surface. Similar defects were observed to form in five of the twelve layers. The surface contamination could be detected on the following layer using the coaxial system. The integrated intensity feature was shown to have highest feature importance, leading to a drop in detection performance of 77%. The work highlights the ability of the system to detect both identified failure modes, suggesting in-situ monitoring systems can observe both spatter defect initiation and surface contamination. This is important to enable robust detection systems. In future, the impact of spatter defects on material properties should be characterised and more failure mechanisms should be explored such as keyhole porosity detection. Furthermore, uncertainty in the measurement should be quantified by studying the performance on a larger dataset.

References

[1] Larsen, S., & Hooper, P. A. 2022 *Journal of Intelligent Manufacturing*, **33.2**, 457-471
[2] Gobert, C., Reutzel, E. W., Petrich, J., Nassar, A. R., & Phoha, S. 2018 *Additive Manufacturing,* **21**, 517-528.
[3] Petrich, J., Snow, Z., Corbin, D., & Reutzel, E. W. 2021 *Additive Manufacturing*, **48**, 102364.
[4] Hooper, Paul A. 2018 *Additive Manufacturing* **22** 548-559.
[5] Larsen, S., & Hooper, P. A. 2023 *Manuscript submitted for publication.*
[6] Larsen, S., & Hooper, P. A. 2023 *arXiv preprint* arXiv:2305.02695.
[7] Breiman, L. (2001). Random forests. *Machine learning*, **45**, 5-32.